PAPER

Check for updates

Drone-based particle monitoring above two harmful algal blooms (HABs) in the USA†

Landon Bilyeu, [ID] [a] Bryan Bloomfield,[a] Regina Hanlon, [ID] [a] Javier González-Rocha, [ID] [ab] Stephen J. Jacquemin,[c] Andrew P. Ault, [ID] [d] Johnna A. Birbeck,[e] Judy A. Westrick, [ID] [e] Hosein Foroutan, [ID] [f] Shane D. Ross, [ID] [b] Craig W. Powers[ab] and David G. Schmale, III [ID] *[a]

Little is known about the transport and fate of aerosolized particles associated with harmful algal blooms (HABs). An Airborne DROne Particle-monitoring System (AirDROPS) was developed and used to monitor, collect, and characterize airborne particles over two HABs in Grand Lake St Marys (GLSM) and Lake Erie (LE), Ohio USA in August 2019. The AirDROPS consisted of an impinging device (ID) and an optical particle counter (OPC) mounted on a large commercial quadcopter (DJI Inspire 2). The sensor package was mounted above the airframe to limit the effects of propeller downwash that can corrupt measurements taken below the drone. Nineteen flights were conducted 10 m above water level (AWL) at GLSM, and five flights were conducted 10 m AWL at LE. The sampling height was chosen to minimize the effects of propwash on aerosolization from the lake surface. One intercomparison flight was conducted at GLSM over land adjacent to a sonic anemometer mounted on the top of a flagpole 15 m above ground level (AGL). Particle counts generally decreased from morning to afternoon flights, ranging from >4000 in the morning to <1000 later in the day. Decreased particle counts were associated with an increase in windspeed that corresponded with time of day, ranging from >4000 below 4 m s^{-1} to <2500 above 4 m s^{-1}. Flow cytometry was used to image particles trapped in a liquid impinger onboard the AirDROPS. Sixty percent (15/25) of the impinger samples contained at least one biotic (fluorescent) object. Impinger samples were also analyzed for a suite of potential cyanotoxins using liquid chromatography-mass spectrometry (LC-MS/MS), but no cyanotoxins were detected in any of these air samples (water samples collected during a similar time contained greater than 20 μg L^{-1} microcystins). Additional work is needed to understand the environmental factors associated with the potential aerosolization and transport of cyanobacterial cells and toxins in aquatic environments.

Environmental significance

Harmful algal blooms (HABs), caused mostly by toxin-producing cyanobacteria, may have negative health impacts on surrounding communities. Little is known about the fate and transport of the aerosolized HAB organisms and associated toxins, and to what extent weather conditions influence the movement of these into the atmosphere. By measuring particle counts above an active HAB site, we were able to show correlations between weather effects with the number of particles measured above the HAB. We were able to utilize this data to create a model that could predict the particle count using weather conditions. While our model was made using only one lake system, the methods could be applied to other freshwater HABs.

[a]*School of Plant and Environmental Sciences, Virginia Tech, Blacksburg, VA, USA. E-mail: dschmale@vt.edu; Fax: +1-540-231-7477; Tel: +1-540-231-6943*

[b]*Department of Aerospace and Ocean Engineering, Virginia Tech, Blacksburg, VA, USA*

[c]*Wright State University – Lake Campus, 7600 Lake Campus Drive, Celina, OH, USA*

[d]*Department of Chemistry, University of Michigan, Ann Arbor, MI, USA*

[e]*Lumigen Instrumentation Center, Department of Chemistry, Wayne State University, Detroit, MI, USA*

[f]*Department of Civil and Environmental Engineering, Virginia Tech, Blacksburg, VA, USA*

† Electronic supplementary information (ESI) available. See https://doi.org/10.1039/d2ea00055e

1 Introduction

Harmful algal blooms (HABs), caused mostly by toxin-producing cyanobacteria, occur naturally in freshwater systems.[1–3] HABs form as a result of lake conditions favorable to cyanobacterial growth, such as high levels of phosphorus and warmer temperatures.[4] These conditions can occur in areas with high agricultural runoff and are a particular risk to shallow waters. HABs are often associated with high levels of cyanotoxins that pose a significant health threat to humans and domestic animals.[5–7] The exposure of HAB associated aerosols

© 2022 The Author(s). Published by the Royal Society of Chemistry

Environ. Sci.: Atmos., 2022, **2**, 1351–1363 | 1351

has been shown to pose health threats using *Drosophila melanogaster* as an animal model.[8] Furthermore, HABs appear to be increasing in freshwater bodies around the world.[4,9]

Research is needed to mitigate HABs, including the development of new low-cost and turn-key technologies to capture, detect, and quantify HAB cells and toxins in water and air.[3,4] Water samples suspected to contain HABs are usually collected by hand from crewed boats and shipped to off-site laboratories for cyanotoxin analyses. Detailed cyanotoxin analyses are usually conducted using liquid chromatography coupled with tandem mass spectrometry (LC-MS/MS), but the high costs of these instruments preclude their widespread use. Commercially available enzyme linked immunosorbent assays (ELISAs) are common for some cyanotoxins such as microcystins (MCs), employing either monoclonal or polyclonal antibodies.[6] New low-cost technologies with quick turn-around times are needed to understand threats, manage risks, and mitigate incidents associated with HABs.

Grand Lake Saint Marys (GLSM) is a natural HAB laboratory; the lake has experienced a recurring HAB since 2010.[10] LE has also experienced several significant HABs in recent years. A HAB in 2014 near the water treatment plant intake for Toledo, OH led to non-potable water for days.[11] HABs on LE are often associated with the southern and western portions of the lake, likely stemming from increased nutrient input from the Maumee River.[12] Similar to GLSM, LE has been experiencing HABs for at least the past few decades, due in large part to the highly agricultural watershed and resulting nutrient rich runoff coupled with the shallow depth and bathymetry of the lake.[13]

Lakes with HABs have been shown to produce lake spray aerosols (LSAs) through the breaking of waves and the bursting of bubbles.[14,15] These processes may release HAB-associated particles into the air above the lake surface.[16] Red tides in the ocean are known to produce aerosolized toxins known as brevetoxins that may irritate the eyes and lungs of humans.[17] Though red tides have been the focus of a considerable amount of research in the past decade,[18] relatively little is known about the airborne transport and fate of freshwater HABs and their associated toxins. This information is critical for health advisories issued *via* water quality experts, and for the communities of people that live on or around contaminated bodies of water.[19]

A number of different techniques and approaches have been used to study the aerosolization and transport of microorganisms from aquatic environments. May *et al.* (2016)[15] developed a chamber to study LSA generation under controlled environmental conditions. Pietsch *et al.* (2018)[16] used a thin tank to study wind-induced aerosolization of the bacterium *Pseudomonas syringae*. Harb *et al.* (2019)[20] used a chamber to study the potential impact of salinity on the aerosolization of microorganisms from aquatic environments. Powers *et al.*[21] developed an extensive sampling tower for an uncrewed surface vehicle (USV) to collect microorganisms and monitor particle sizes in the atmosphere above a salt pond in Falmouth, MA, USA and a freshwater lake in Dublin, VA, USA. The bioaerosol-sampling system featured in that work included a series of 3D-printed impingers, two different optical particle counters, and a weather station. A small, uncrewed aircraft system (sUAS;

a fixed-wing drone) was used in a coordinated effort with the USV to collect microorganisms 50 m above the surface of the water. Samples from the USV and sUAS were cultured on selective media to estimate concentrations of culturable microorganisms. In this manuscript, we extend these prior efforts to the development and use of a unique Airborne DROne Particle-monitoring System (AirDROPS) to collect and characterize aerosols directly over HABs in two freshwater lakes. The AirDROPS consisted of low-cost and lightweight sensors, including an impinging device (ID) and an optical particle counter (OPC) mounted above a large commercial quadcopter (DJI Inspire 2). The OPC used on the AirDROPS can characterize particles up to 10 μm, which is above the size range of cells of *Microcystis* which have been reported to be 1–7 μm.[14] Laboratory calibration experiments were conducted to assess the reliability of the OPCs after a period of use.[22,23] We hypothesized that particle size distributions above two freshwater HABs would be associated with windspeed, wind direction, and temperature. The specific objectives of our work were to: (1) design an automated drone-based sampler to monitor particle sizes in the atmosphere and collect HAB cells and toxins, (2) use the drone-based sampler to monitor the distribution of particles in the atmosphere directly above two freshwater HABs, and (3) observe potential associations of wind direction, windspeed, and temperature with particle counts from the drone-based sampler.

2 Materials and methods

2.1 Study sites

GLSM is an artificial lake in western Ohio with a surface area of 54.6 square kilometers and average depth of about 2 m.[10] In the GLSM watershed, over 90% of the land use is row crops or pastureland which leads to a high amount of nutrient pollution into the lake.[24] The shallow lake warms to between 20 and 30 °C in the summer months.[11] The warmer waters and higher nutrient load in the lake allow the cyanobacteria to outcompete other algae in the lake, creating a bloom of toxin producing cyanobacteria. Samples were collected over five consecutive days between 5–9 August 2019 at GLSM and LE in Ohio, USA (LE). Drone sampling missions were conducted 10 m above the water surface at coordinates 40.544074, −84.508220 (Table 1) in order to obtain unique measurements of collected aerosols and particle counts at heights above the water surface that could not be reached by boat. Wind speed and direction were collected by an anemometer attached to a flagpole at coordinates 40.544035, −84.508114. Due to the lack of an unobstructed space to place the stationary wind sensor at LE (there were tall trees at the sampling location that obstructed the sampling domain), wind data were collected through a separate drone flown simultaneously 10 m above the water. Wind data from these flights were gathered using previously published methods where the motion of the drone was used to infer windspeed and wind direction.[25,26] One of the flights at GLSM was also used for comparison with a concurrent separate drone flight measuring wind conditions and was flown adjacent to a sonic anemometer mounted on the top of a 15 m flagpole (Flight 20, Table 1).

Table 1 Details on AirDROPS sampling missions at GLSM and LE. AirDROPS was used to collect and characterize particles over two HABs. The AirDROPS consisted of an impinging device and an optical particle counter mounted above a large commercial quadcopter. Nineteen flights were conducted 10 m above water level (AWL) at GLSM, and five flights were conducted 10 m AWL at LE. One sensor intercomparison mission (flight 20) was conducted over land adjacent to a sonic anemometer mounted on the top of a flagpole 15 m above ground level (AGL)

Flight #	Lake	Mission	Date	Start time (ET)	Stop time (ET)	Sample time (min)	Height above water (m)	GPS of sampling location	OPC count per mL	Red channel obj per mL
1	GLSM	Sample above lake surface	5-Aug-19	8:04 AM	8:17 AM	13	10	40.544873, −84.510843	45.3	0.0
2	GLSM	Sample above lake surface	5-Aug-19	9:07 AM	9:17 AM	10	10	40.544873, −84.510843	51.1	413.5
3	GLSM	Sample above lake surface	5-Aug-19	10:09 AM	10:19 AM	10	10	40.544873, −84.510843	29.4	0.0
4	GLSM	Sample above lake surface	5-Aug-19	11:06 AM	11:16 AM	10	10	40.544873, −84.510843	21.2	0.0
5	GLSM	Sample above lake surface	5-Aug-19	12:03 PM	12:13 PM	10	10	40.544873, −84.510843	22.1	0.0
6	GLSM	Sample above lake surface	5-Aug-19	1:05 PM	1:15 PM	10	10	40.544873, −84.510843	22.1	0.0
7	GLSM	Sample above lake surface	5-Aug-19	2:07 PM	2:17 PM	10	10	40.544873, −84.510843	16.3	871.4
8	GLSM	Sample above lake surface	5-Aug-19	3:03 PM	3:14 PM	11	10	40.544873, −84.510843	11.2	461.2
9	GLSM	Sample above lake surface	6-Aug-19	8:10 AM	8:20 AM	10	10	40.544873, −84.510843	54.5	2535.1
10	GLSM	Sample above lake surface	6-Aug-19	9:06 AM	9:16 AM	10	10	40.544873, −84.510843	36.4	3984.5
11	GLSM	Sample above lake surface	6-Aug-19	10:04 AM	10:14 AM	10	10	40.544873, −84.510843	18.9	n.d.
12	GLSM	Sample above lake surface	6-Aug-19	10:36 AM	10:46 AM	10	10	40.544873, −84.510843	19.1	0.0
13	GLSM	Sample above lake surface	6-Aug-19	11:07 AM	11:17 AM	10	10	40.544873, −84.510843	23.1	0.0
14	GLSM	Sample above lake surface	6-Aug-19	11:35 AM	11:42 AM	7	10	40.544873, −84.510843	17.3	0.0
15	GLSM	Sample above lake surface	6-Aug-19	12:43 PM	12:53 PM	10	10	40.544873, −84.510843	11.5	0.0
16	GLSM	Sample above lake surface	6-Aug-19	1:06 PM	1:16 PM	10	10	40.544873, −84.510843	35.7	0.0
17	GLSM	Sample above lake surface	6-Aug-19	1:34 PM	1:44 PM	10	10	40.544873, −84.510843	0.0	2030.8
18	GLSM	Sample above lake surface	6-Aug-19	2:06 PM	2:16 PM	10	10	40.544873, −84.510843	0.0	853.6
19	GLSM	Sample above lake surface	6-Aug-19	2:37 PM	2:47 PM	10	10	40.544873, −84.510843	0.0	2518.2
20	GLSM	Sensor calibration	7-Aug-19	8:18 AM	8:28 AM	10	15	40.544074, −84.508220	0.0	831.1
21	LE	Sample above lake surface	8-Aug-19	11:36 AM	11:46 AM	10	10	41.702472, −83.463598	5.54	2737.2
22	LE	Sample above lake surface	8-Aug-19	12:07 PM	12:17 PM	10	10	41.702472, −83.463598	5.68	5817.6
23	LE	Sample above lake surface	8-Aug-19	1:07 PM	1:17 PM	10	10	41.702472, −83.463598	5.37	2509.8
24	LE	Sample above lake surface	8-Aug-19	1:37 PM	1:47 PM	10	10	41.702472, −83.463598	5.38	2578.4
25	LE	Sample above lake surface	8-Aug-19	2:09 PM	2:14 PM	5	10	41.702472, −83.463598	5.21	2535.1

2.2 Airborne drone particle-monitoring system

The AirDROPS was designed and deployed for sampling bioaerosols and monitoring particle size distributions. The sampler was constructed using a 38.5 mm diameter by 290 mm length PolyPropylene tube and Polylactic Acid 3D printer components (Fig. 1A). The sampler was mounted on top of the drone airframe (Fig. 1B) to limit the effects of propeller downwash that can corrupt measurements taken below the drone.[27,28] The sampler was powered *via* a single 3.7 V 3000 mA h 15 A lithium-ion battery (Samsung 30Q INR 18650) that was changed out with every flight. An impinger was designed using a stainless-steel tube and PolyCarbonate 3D printed components to allow for high temperature sterilization by autoclave and field

Fig. 1 (A) Engineering model of the AirDROPS package. (B) The AirDROPS attached to the DJI Inspire 2 platform. (C) Intercomparison flight of the AirDROPS adjacent to the sonic anemometer mounted on the flagpole. (D) Sampling mission at GLMS, 10 m above the surface of the water. (E) Drone image and aerial view of the sampling location at LE to the right of the point in the image.

disinfection using ethanol. The impinger was based on a design previously described by Powers *et al.*, 2018 [21] adapted for use with a 15 mL polypropylene sterile conical centrifuge tube (CLS430791, Corning, Millipore Sigma). An aliquot of 2.5 mL of sterile water was added to the 15 mL conical tube immediately prior to each sampling mission. Two micro vacuum pumps (PN: SC3101PM, 21 Hualun Sci & Tech Pk 1st Ind Zn Fenghuang Village, Fuyong Town, Shenzhen, Guangdong, China) were used in parallel to supply a flow rate of 0.6 L min^{-1} to the impinger. This flow rate was determined using an FTS Flow Calibrator from ARA Instruments (Eugene, OR, USA), and was optimized to ensure that the impinging fluid was not evacuated from the tube during the sampling mission (*i.e.*, higher flow rates caused water to escape the tube into the vacuum pump). The collection efficiency of the impinger has been reported previously by Powers *et al.*[21] to be 75% for 1 μm polysterene latex beads and 99% for 3 μm polysterene latex beads. The inlet to the impinger was located 330 mm above the horizontal plane of the drone propellers to limit fouling of the sensor due to propwash (Fig. 1B). An optical particle counter (PMS7003, Plantower,

Shunyi District, Beijing, China) was used to record six particle size bins, each greater than 0.3, 0.5, 1.0, 2.5, 5.0, and 10.0 μm. PM_1, $PM_{2.5}$, and PM_{10} numbers were calculated internally by the PMS7003. The inlet to PMS7003 sensor was located 312 mm above the horizontal plane of the drone propellers (Fig. 1B). An environmental sensor (BME280, Bosch Sensortec GmbH, Gerhard-Kindler-Strasse 9, 72 770 Reutlingen Germany) was used to measure ambient temperature, relative humidity, and barometric pressure. The BME280 was located 132 mm above the horizontal plane of the drone propellers. A GPS module (GPS-13740, SparkFun Electronics, 6333 Dry Creek Parkway, Niwot, CO 80503) was used for location and time data. All available data was recorded by the ARM-based microcontroller to a secure digital (SD) card at 1 Hz. The combined weight of the AirDROP including a battery and a 15 mL conical tube with 2.5 mL of sterile water was 587 g. This is below the safe limit operations of the Inspire 2 platform payload, which the manufacturer has specified as no greater than 810 g.[29] With the AirDROPS installed, the Inspire 2 platform had a reasonable (safe) flight time of about 15 minutes. Our sampling missions

were designed with this limit in mind (10 minutes), providing enough time for takeoff, transit to and from the sampling location, and return to home for landing (about two minutes, given the location of our takeoff and landing spot).

2.3 Flight operations

For each sampling mission, the AirDROPS was flown into position, and held in 'Positioning mode' at a constant altitude of 10 m above the lake surface (Fig. 1D). This height was chosen to reduce the impact of downwash on the lake surface as well as to measure aerosol levels higher above the HAB source than had been done previously using watercraft. The sensor package was powered on using a photoelectric switch mounted over the left rear green LED light on the Inspire 2. The lights were powered on in the DJIGO4 app, starting the sensor package over water once the drone was in the correct position. The sensor package remained on for a period of 10 min. After 10 min, the sensor package was powered off using the photoelectric sensor, and the drone was returned home for landing.

2.4 Flow cytometry of impinger samples collected 10 m above the HABs

The concentration of impinged particles from the atmosphere above freshwater lake sites was determined with an Imaging Cytometer (Amnis ImageStream MarkII). The impinged aerosols were counted as obj per mL at $60\times$ magnification in both the brightfield (BF) (457/45 nm bandpass filter) and red channels (642 nm excitation and 702/86 nm emission wavelength) (Fig. 2). Phycocyanins are the light harvesting pigments found in cyanobacteria and these pigments are optimally excited in the red range with an emission spectrum that can be captured between 630 nm and 800 nm. Samples were stored at -20 °C, thawed, and equilibrated at room temperature, prior to being run. One mL of the impinged liquid sample was spun twice at $3000\times$ gravity for five minutes. Two aliquots of 42 μL were immediately recovered from the liquid near the bottom of the tube, with care to avoid any debris on the tube bottom. Molecular biology grade water was filtered with a 0.2 μm filter and used as a blank in the machine before running samples.

Due to the predicted low number of putative captured biotic aerosols, a 3 min run time was standardized for each impinged sample. In a previous study with natural and simulated rain, samples were run for three min to obtain obj per mL outputs.[21] These authors determined that 3 min sample runs showed similar size distributions relative to samples that reached 1000 obj per mL in less than three min, and the background level of bacteria in the nucleic acid staining dye in sterile control water was 297 ± 82 DNA-containing particles per 10 μL ($n = 3$). We did not use a nucleic acid staining dye in this study. Instead, the total obj per mL data for biotic particles was captured in the red channel to eliminate abiotic debris that might give rise to a false count in the BF channel alone. The objects counted in the red channel were considered to be biotic in origin, regardless of fluorescence level. Sample run focusing was achieved with SpeedBead® reagent beads (Amnis Cat. #400040) during data acquisition. The beads were removed by gating before object

counts were generated for each run. To obtain total aerosolized particles captured, the BF channel data was corrected by subtraction of particles within the SpeedBead capture range. These counts were sorted by the size of the objects into bins of 0.13–1.13, 1.13–1.60, 1.60–1.95, 1.95–2.76, 2.76–3.91, 3.91–5.64, 5.64–6.91, 6.91–7.98, and 7.98–8.92 μm radius objects. The radius was calculated using the total size of the objects and assuming a circular (spherical) shape.

To calculate the total number of aerosolized particles collected during each impinger collection, the average of the total BF obj per mL for the zero red channel runs were assigned to a discrete size bin. The mean of this total obj per mL (for each size bin) was subtracted from the corresponding total BF obj per mL (for each size bin) for each run that contained a positive fluorescent object in the red channel. By subtracting the average particle count data for samples with zero objects in the red channel, from those with red objects, we were able to normalize by correcting for abiotic debris particle capture.

2.5 Cyanotoxin analyses using LC-MS/MS

Toxins from cyanobacteria were detected using LC-MS/MS methods described in Birbeck et al. 2019.[30] Sample analytes were loaded into a Thermo Scientific TSQ Altis™ triple quadrupole mass spectrometer (Thermo Scientific, Waltham, MA, USA) with an EQuan MAX Plus™ system and then separated on a Thermo Accucore aQ, 50 × 2.1 mm, 2.6 μm particle size column. A standard curve was prepared between 0.5–500 ng L^{-1}, with detection limits for MCs and nodularin being between 0.5–10 ng L^{-1}. An electrospray ionization source was used in positive ion mode. Additional details regarding these methods are provided in Hanlon et al. (2022)[31] and reference ions are provided in Table 1.† The TraceFinder™ EFS 4.1 software package was used to ensure proper cyanotoxin identification (Table 1†).
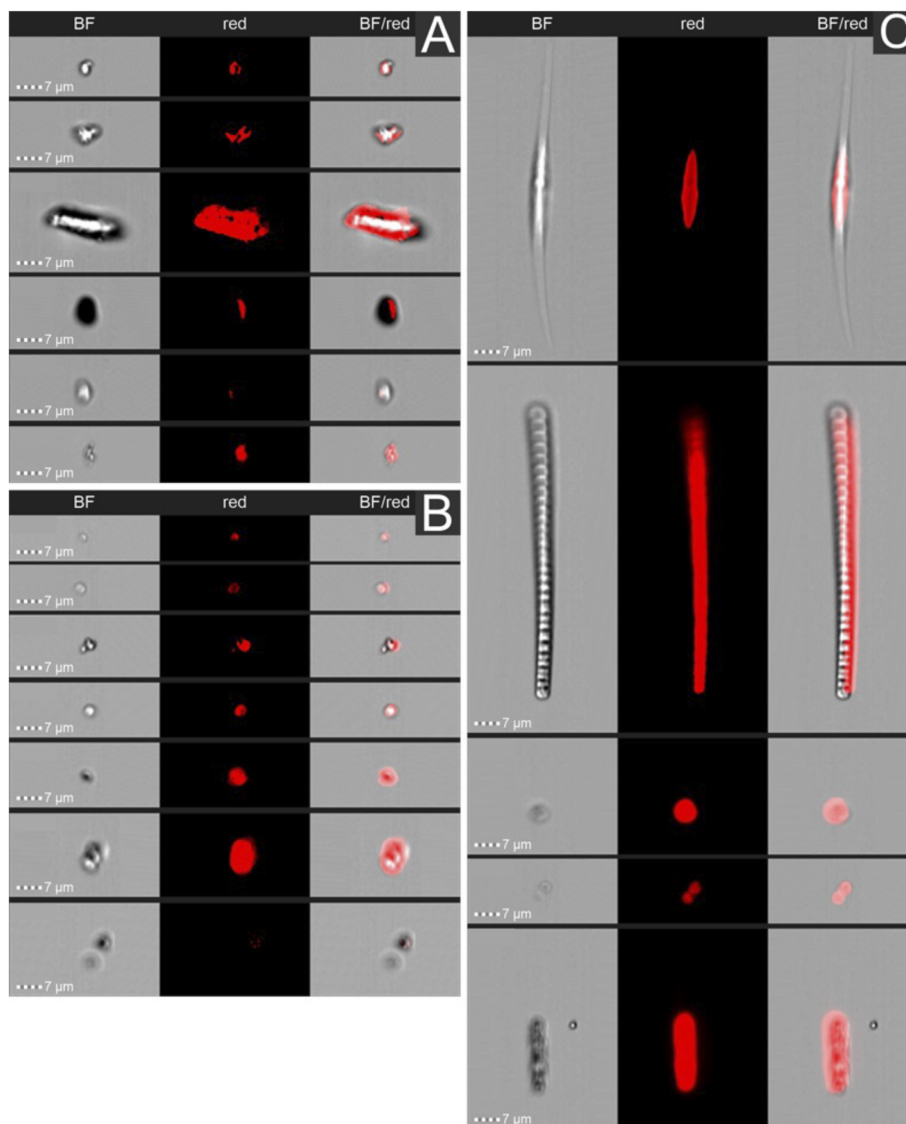
2.6 Particle counts 10 m above the HABs

The PMS7003 was used to count particles six particle size bins, each greater than 0.3, 0.5, 1.0, 2.5, 5.0, and 10.0 μm diameter in 0.1 L of air, and had a sample rate of about 1 Hz. The sampling occurred over 10 min intervals in tandem with the drone-based impinger. Airborne particle counts were measured according to the times shown in Table 1. The data collected was saved to an SD card in comma-separated values (CSV) file format and transferred before clearing the SD card to prepare for the next flight.

2.7 Ground-based measurements of windspeed and wind direction

At GLSM, an Atmos 22 sonic anemometer weather station was aligned north with a compass and raised on a flagpole to a height of 15 m where it recorded wind speed and direction measurements every 15 s. Data were saved to an SD card and collection was run from 8:00 until 16:00 local time, daily. The same ground-based anemometer was also used at LE, but trees obstructed this sensor during flight operations so local wind data for the LE flights were determined from drone-based

© 2022 The Author(s). Published by the Royal Society of Chemistry

Environ. Sci.: Atmos., 2022, **2**, 1351–1363 | **1355**

Fig. 2 Selected images from flow cytometry analyses of impinger samples from the AirDROPS. (A) Objects from an impinger sample collected above GLSM showing brightfield, red filter, and combination of the two. (B) Objects from an impinger sample collected above LE showing brightfield, red filter, and combination of the two. (C) Objects from a lake water sample from LE showing brightfield, red filter, and combination of the two.

measurements of wind.[32] These measurements were taken every second and matched with the time recorded on the AirDROPS to align particle count measurements with the wind speed and direction calculations.

2.8 Drone-based wind velocity measurements

Drone-based wind velocity measurements were derived from a 3DR Solo quadrotor using the model-based wind estimation technique described in (González-Rocha et al., 2019; 2020).[25,26] With this method, wind velocity is inferred from wind-induced vehicle motion perturbations experienced as the drone sustains hovering flight. The general accuracy of this drone-based wind sensing approach has been demonstrated through previous experiments where drone, sonic anemometer, and a Sonic

Detection and Ranging instrument (SoDAR) wind velocity measurements have been compared at various heights above ground level.[25–27]

2.9 Optical particle counter calibration experiments

The initial OPC calibrations were done according to the procedure outlined in Powers et al., 2018.[21] The accuracy of the OPC used onboard the AirDROPS was assessed in a series of controlled laboratory experiments against an Aerodynamic Particle Sizer (APS, Model 3321, TSI Incorporated, Shoreview Minnesota, USA). Briefly, particles of known sizes (1 and 3 microns) were released into a sealed bag and measurements from the OPC were compared to the APS.

2.10 Data analyses

Data were saved in CSV files and were trimmed and aligned in Microsoft Excel. Statistical analyses were performed with JMP Pro Version 17 software (Cary, North Carolina, USA). A model was fit using the JMP neural network to create a prediction equation for GLSM which utilized wind speed, wind direction, and temperature to predict the particle count. The neural network weighs inputs from a provided dataset to create a prediction equation that will estimate a specific output parameter. The model was set up to create three hidden node equations that combine into an overall theta equation. The theta equation predicts the particle count from the provided weather data. The program adjusts the values in the hidden node equations and overall theta equation until it fits the best curve to the data.[33,34] To get the best fit, the model was trained using all of the data collected from the sampling periods of August 5th and August 6th, 2019 for which we had both weather data and particle counts. The model was trained with a randomly selected 2/3[rds] of the collected data, and utilized the remaining 1/3rd as verification for the prediction equation. This resulted in 368 measurements to train the model, and another 184 to verify the model.

3   Results

3.1   Flights

Twenty flights were conducted at GLSM, and five flights were conducted at LE (Table 1). Twenty-four of the flights were conducted 10 m above the surface of the water (Table 1). One of the flights at GLSM was used to calibrate the drone sensor package (Flight 20, Table 1), and was flown adjacent to a sonic anemometer mounted on the top of a flagpole (Fig. 1C).

3.2   Wind direction and wind speed

The wind direction was consistent across the lakes and toward the shore-based operations for all the sampling missions performed at the two lakes (Fig. 1 and 4). For GLSM, the sonic anemometer (mounted on the flagpole) recorded wind speeds from 0–10 m s^{-1} (Fig. 4), and wind directions ranging from a source of 150–300° (Fig. 3. At GLSM, windspeed increased from morning to afternoon flights (Fig. 4)). At LE, windspeed was variable and ranged from 1 to 12 m s^{-1} across all sampling missions (Fig. 4).

3.3   Particle counts

At GLSM, airborne particle counts generally decreased from morning to afternoon flights (Fig. 5). We observed decreased particle counts at GLSM associated with an increase in windspeed from morning to afternoon (Fig. 6). For the size bin of 0.3–0.5 μm diameter, particle counts per 0.1 L of air ranged from about 1000 (afternoon flights) to 4000 (morning flights) per measurement (Fig. 5). For the size bin of 0.5–1.0 μm diameter, particle counts ranged from about 300 (afternoon flights) to 1500 (morning flights) per measurement (Fig. 5). For the size bin of 1.0–2.5 μm diameter, particle counts ranged from about 30 (afternoon flights) to 250 (morning flights) per
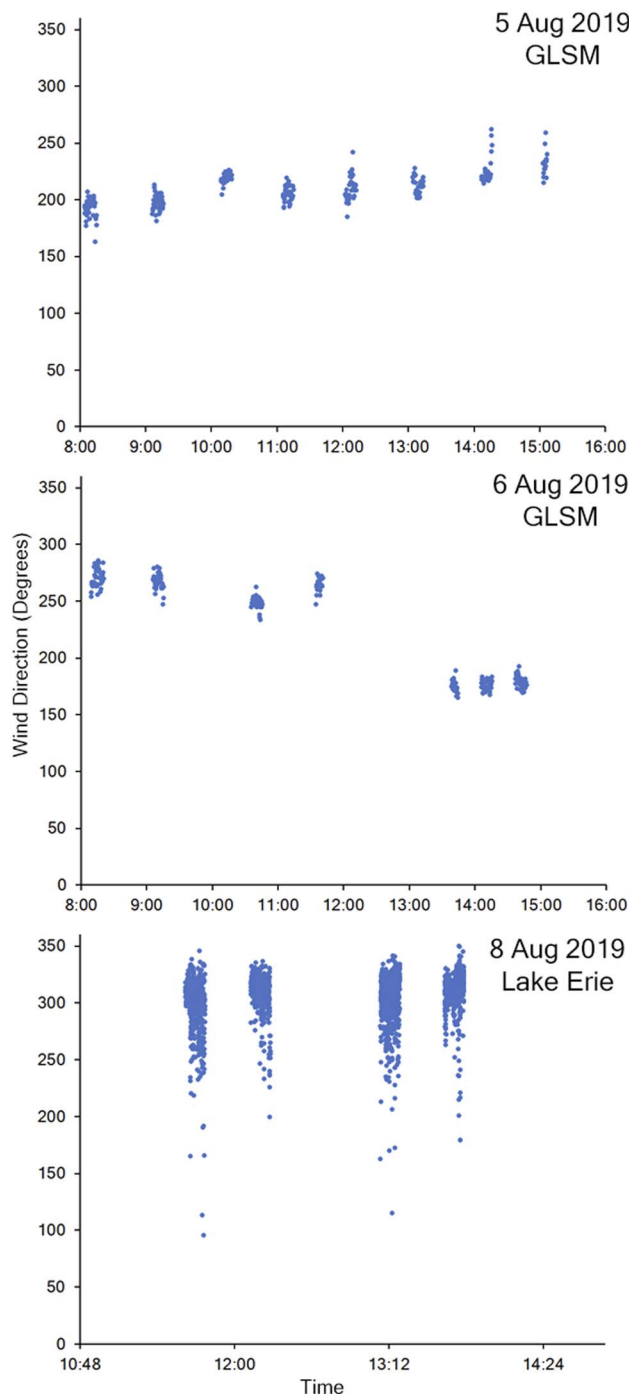

Fig. 3 Wind direction (degrees) over the course of the day. The first two graphs represent August 5th to 6th, 2019 at GLSM. The third graph represents August 8th, 2019 at LE. The wind direction was determined using a sonic anemometer for August 5th to 7th, 2019, and using GLOS data for August 8th, 2019.

measurement (Fig. 5). For larger size bins (2.5–5.0, 5.0–10.0, and 10.0+ μm), particle counts ranged from 0 to 30 per measurement (Fig. 5).

At LE, airborne particle counts were generally lower than GLSM and consistent from morning to afternoon flights (Fig. 5). At the time LE was not experiencing an algal bloom at the

Fig. 4 Wind speed (m s^{-1}) over the course of the day. The first two graphs represent August 5th to 6th, 2019 at GLSM. The third graph represents August 8th, 2019 at LE. The wind speed was determined by our sonic anemometer for August 5th to 7th, 2019, and using GLOS data for August 8th, 2019.

severity of the one in GLSM, which could have contributed to the lower particle counts. There was no association with particle counts with windspeed (Fig. 6). For the size bin of 0.3–0.5 μm diameter, particle counts ranged from about 400 to 700 per measurement (Fig. 5). For the size bin of 0.5–1.0 μm diameter,

particle counts ranged from about 100 to 300 per measurement (Fig. 5). For the size bin of 1.0–2.5 μm diameter, particle counts ranged from about 20 to 35 per measurement (Fig. 5). For larger size bins (2.5–5.0, 5.0–10.0, and 10.0+ μm), particle counts ranged from 0 to 2 per measurement (Fig. 5).

At GLSM when looking at particle counts over time, we saw the particle count decrease significantly as the day went on, dropping to as little as 1/6th the morning particle count levels (Fig. 5). During our sampling throughout the day. The wind-speed increased by 2 to 3 times the morning speed (Fig. 4), but the wind direction only slightly shifted and was always coming from off the lake. At LE, we saw lower average particle counts than at GLSM but had similar wind source distribution with over 90 percent of wind source direction coming from between 270 and 360° which was off the lake.

3.4 Flow cytometry and cyanotoxin analyses of impinger samples

Selected panels of fluorescent objects present in the impinger samples are shown in Fig. 2. Sixty percent (15/25) of the impinger samples contained at least one biotic (fluorescent) object, ranging from 1 to 7 obj per mL (Fig. 2). Total biological objects counted in the R1 channel were sorted by size with the majority falling between 1.95 and 3.91 μm (Fig. 7). When comparing total particle counts and object concentrations, no association was observed (Table 1). However, despite lower particle counts at LE there were larger numbers of objects observed in the impinger (Table 1). Impinger samples were also analyzed for a suite of cyanotoxins using LC-MS/MS, but no cyanotoxins were detected in any of the samples. Water samples collected during a similar time contained greater than 20 μg L^{-1} microcystins.[31]

3.5 Predicting particle counts as a function of environmental parameters

Particle counts >0.3 μm from August 5 were observed as a function of wind speed, wind direction, and temperature (Fig. 8). Fig. 8 shows the actual measured particle counts plotted against the model predicted versions which results in an optimized model with a R Square of 0.87 and a validation prediction with a R Square of 0.86. The hidden node equations and overall prediction equation, are as follows:

$$H1 = \tanh(0.500 \times (0.257 \times \text{Wind\_Speed\_ms} - 0.002 \times \text{Wind\_Direction\_Deg} + 0.545 \times \text{Temperature\_C} - 14.133));$$

$$H2 = \tanh(0.500 \times (0.143 \times \text{Wind\_Speed\_m\_s} + 0.004 \times \text{Wind\_Direction\_Deg} + 1.269 \times \text{Temperature\_C} - 34.909));$$

$$H3 = \tanh(0.500 \times (-0.308 \times \text{Wind\_Speed\_ms} - 0.009 \times \text{Wind\_Direction\_Deg} - 0.115 \times \text{Temperature\_C} + 6.022));$$

$$\text{THETA1} = -3913.359 \times H1 + 881.325 \times H2 - 901.768 \times H3 + 3582.704$$

This model based on a neural network allowed for a prediction of the particle counts in the air above the HAB based on weather conditions.
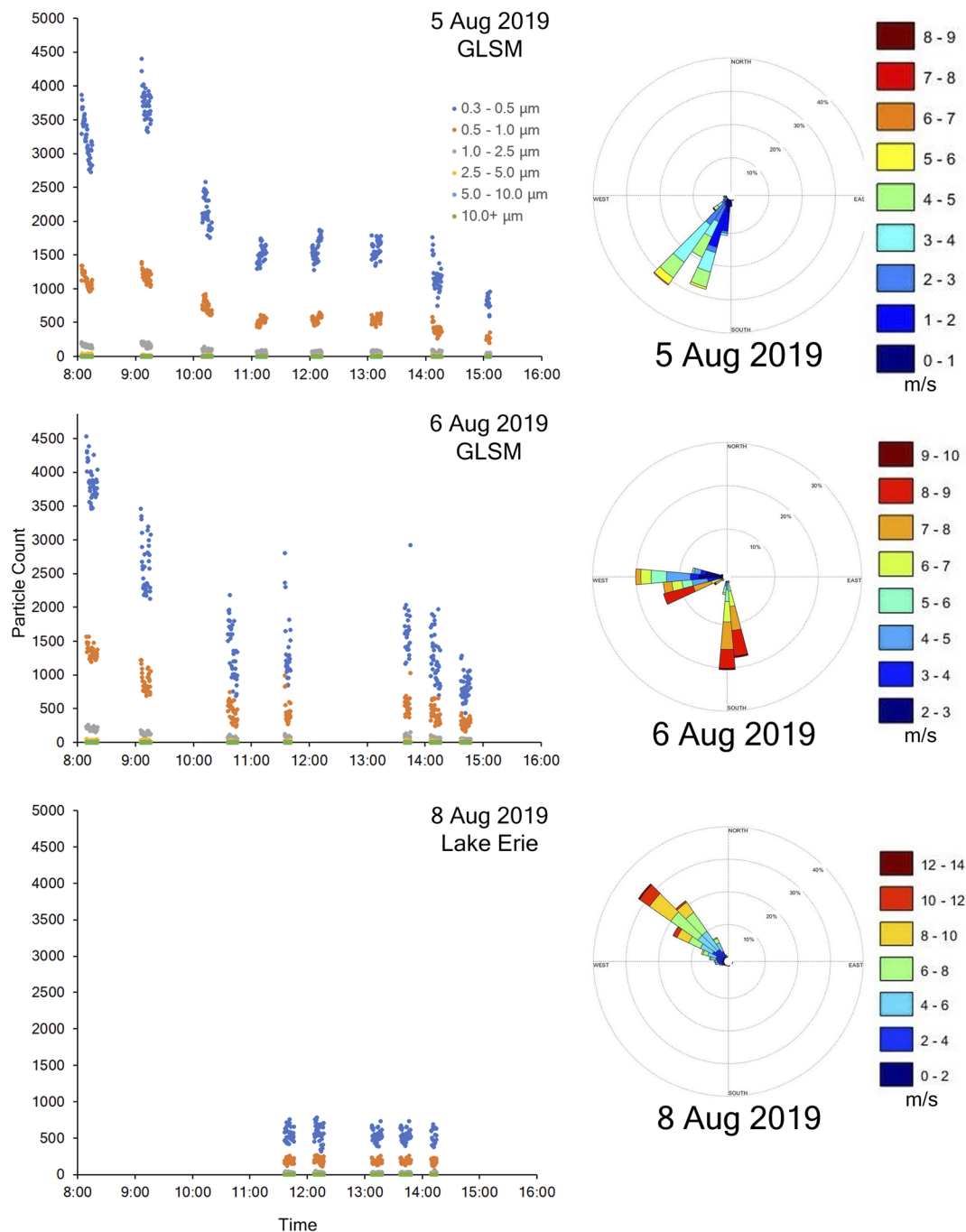
1358 | *Environ. Sci.: Atmos.*, 2022, **2**, 1351–1363

© 2022 The Author(s). Published by the Royal Society of Chemistry

Fig. 5 Airborne particle counts over the course of the day. Data were recorded from a PMS7003 OPC onboard the AirDROPS. The first two graphs show flights that occurred August 5th to 6th, 2019 at GLSM while hovering 10 m over the water. The third graph depicts the flights on August 8th, 2019 while hovering 10 meters over the water at LE. To the right of each graph is the corresponding wind rose which shows wind direction and speed (m s^{-1}) each day.

4   Discussion

Little is known about the airborne fate and transport of HABs and their associated toxins. To address these knowledge gaps, we developed and deployed an airborne drone particle-monitoring system (AirDROPS) to collect and characterize aerosols directly over HABs in two freshwater lakes (GLSM and LE), each with different size and conditions that impact aerosolization processes. The AirDROPS consisted of an impinging device and an optical particle counter mounted above a large commercial quadcopter. Nineteen flights were conducted 10 m above water level (AWL) at GLSM, and five flights were conducted 10 m AWL at LE. One intercomparison flight was conducted at GLSM over land adjacent to a sonic anemometer mounted on the top of a flagpole 15 m above ground level (AGL). Though airborne concentrations of particles have been reported over water using

© 2022 The Author(s). Published by the Royal Society of Chemistry

Environ. Sci.: Atmos., 2022, **2**, 1351–1363 | **1359**

Fig. 6 Airborne particle counts recorded from the OPC onboard the AirDROPS, and windspeed from the sonic anemometer mounted on a flagpole and drone-modeled data for LE. The first two graphs show flights that occurred August 5th to 6th, 2019 at GLSM while hovering 10 m over the water. The third graph depicts the flights on August 8th, 2019 while hovering 10 m over the water at LE.

Fig. 7 Biological object frequency by size from collected air impinged samples onboard the AirDROPS. The graph depicts object counts sorted by size with radius size bins from 1.60–1.95, 1.95–2.76, 2.76–3.91, 3.91–5.64, 5.64–6.91, 6.91–7.98, and 7.98–8.92 μm. The size bins were determined by assuming a spherical shape and calculating the radius of an object from its recorded size in the flow cytometer.

Fig. 8 Measured *vs.* predicted particle counts used in the best fit model. The graph on the top panel shows the fit of the model on the training set of data, while the graph on the bottom shows the fit of the validation set of data. The model was made using the wind speed, temperature, and wind direction through the JMP Pro neural network modeling. The model was trained on two days of collected data, and verified on a random subset of the collected data that was not used to train the model.

uncrewed boats,[21] to our knowledge, the work described here represents the first drone-based measurements of airborne particle counts directly over HABs.

Airborne particle size distributions varied with increasing windspeed for GLSM. Particle counts generally decreased from
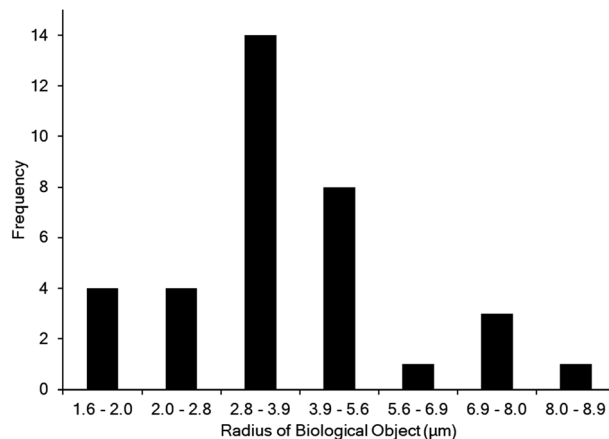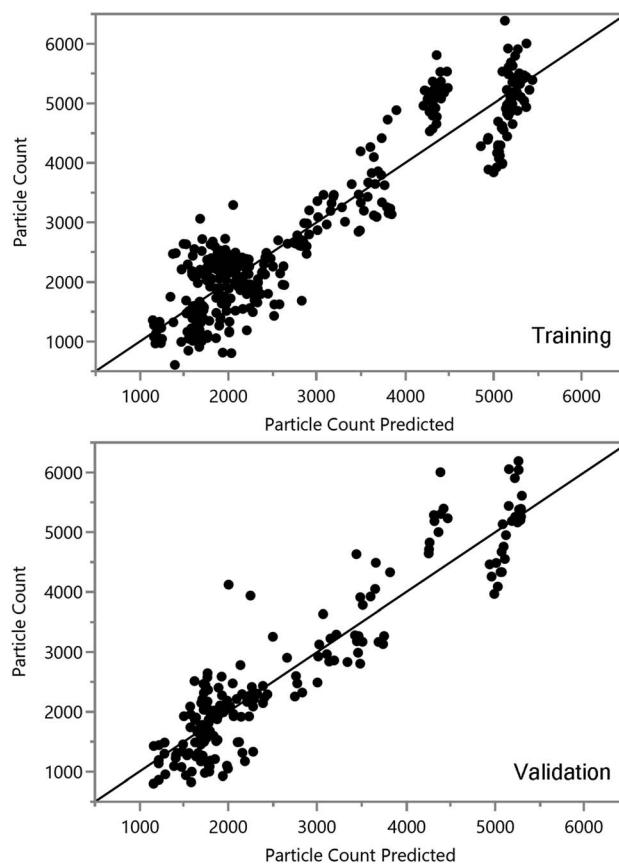
morning to afternoon flights, and the decreased particle counts were associated with an increase in windspeed. In contrast, LE particle counts were much lower, and we did not observe significant trends in particle counts with respect to wind direction, wind speed, or time of day. Airborne particle concentrations have been shown to be associated with windspeed and wind direction above a lake surface.[21] The time of day plays a role in the conditions affecting windspeed and direction through diurnal cycling.[35] In cases of higher windspeeds, it has previously been shown to correlate with a decrease in both fine and course aerosols in the ocean.[36–38] In the case of GLSM, the relatively small size and depth may cause less wave formation and breaking than we would see in large lake spray or sea spray studies, instead likely having aerosol production limited to the surf zone and mechanical disturbances of the surface. LE, however, would be more likely to produce larger numbers of aerosols from wave breaking and bubble-bursting due to the larger size and depth.[14] Previous studies have shown a difference in particle counts with respect to wind direction when it caused a switch from offshore to onshore winds as wind can drive droplet formation from the water surface.[8,39] Our drone sampling missions were conducted exclusively during onshore winds, so consequently we were unable to examine potential associations of particle counts with offshore winds. Since all of our sampling missions were conducted during onshore winds, we speculate that a significant fraction of the observed airborne particles were from the lakes studied. We acknowledge, however, that some of the particles may have originated from other non-lake sources. Future experiments with multiple background sampling locations would help to elucidate potential contributions to airborne particle concentrations.

Sixty percent (15/25) of the impinger samples contained at least one biotic (fluorescent) object. We saw higher numbers on average from LE, which could be caused by lake chemistry or environmental conditions that favor aerosolization of biotic objects.[37,38] Since the biotic objects were often on the larger end of the range (3–10 μm), we speculate that they may have stronger associations with particle counts of those sizes. Unfortunately, due to the low number of particle counts in the larger size bins, we were unable to provide a constructive analysis of this potential association. Impinger samples were also analyzed for a suite of cyanotoxins using LC-MS/MS, but no cyanotoxins were detected in any of the samples. Hanlon *et al.* (2022)[31] conducted a series of water sampling missions at GLSM and LE during the same calendar dates and reported high levels of microcystin in the water, 15.0 and 1.92 μg L^{-1}, respectively. HAB-associated toxins can be aerosolized and transported to inland communities where they threaten the health of humans.[17,18,40–42] In addition, wave breaks and bubble-bursting cause water to spray and contributes to aerosol production and the dispersal of cells, especially in larger bodies of water such as LE,[8] and cyanotoxins into the air.[18] Aerosols produced in this way have been found to contain MCs in samples collected over land near a HAB, showing that the toxin can be transported over land to the surrounding area.[14] Sutherland *et al.*[43] detected anatoxin-a in air samples during a HAB at Capaum Pond on Nantucket Island, Massachusetts, USA in 2019. Though air samples have not yet been incorporated into routine HAB monitoring in freshwater environments, the spread of HAB-associated aerosols in marine environments (*e.g.*, brevetoxin) is known to cause respiratory problems and can be dangerous to those with underlying health conditions.[17] The approach showcased here demonstrates the feasibility of a rapid drone-based system to extend monitoring protocols beyond the water's edge. And while we did not necessarily detect any appreciable toxin values in our samples, our data regarding the distribution of particles as well as impingement of numerous fluorescent objects does validate the approach.

The concerns regarding the accuracy of lightweight and inexpensive OPCs is an important limitation to consider when comparing values of one OPC to another or to determine absolute high or low levels of particles.[22,23] Our field experiments relied on a single OPC as part of the AirDROPS package. However, as shown in the laboratory calibration experiments, the data recorded from this OPC were robust and consistent with simultaneous measurements recorded from the APS.

Additional work is needed to understand the environmental factors associated with the potential aerosolization and transport of cyanobacterial cells and toxins in aquatic environments. Higher windspeeds may decrease total particle counts above a lake, but also drive aerosol production closer to the lake surface.[8,36,44] Though our study was only focused on an altitude of 10 m above the water surface, it sets the stage for future work to examine the vertical distribution of HABs above a lake surface. Powers *et al.*[21] conducted simultaneous sampling missions of microorganisms with a UAS and a USV at Claytor Lake, Virginia, USA. It should be noted that although Claytor Lake had relatively high levels of the bacterium *Pseudomonas syringae*, it was not experiencing a HAB. Additional research is needed to understand threats, manage risks, mitigate incidents, develop capabilities, and strengthen collaborations for improved water quality and security.[3] Aerial and aquatic robots can be fitted with the tools to be used to work alongside health professionals and air and water quality experts to provide critical and timely information to guide regulatory decisions. Modeling of particle counts as a function of the wind speed, wind direction, and temperature could allow for future predictions of areas impacted by HAB-associated aerosols.[39] Such information is critical for determining time-sensitive health advisories, and to create public health forecasting models for the communities of people that live near contaminated bodies of water.

Author contributions

DS conceived, planned, and conducted the field experiments. BB assisted DS with all field experiments and data and sample curation following each sampling mission. LB conducted calibration experiments in the laboratory and analyzed data from all of the experiments. JGR conducted sUAS missions for measurements of wind. RH organized flow cytometry analyses. JB and JW conducted cyanotoxin analyses. LB and DS led the writing of the manuscript. All authors provided feedback on the manuscript.

© 2022 The Author(s). Published by the Royal Society of Chemistry

Environ. Sci.: Atmos., 2022, **2**, 1351–1363 | **1361**

Conflicts of interest

There are no conflicts to declare.

Acknowledgements

References

1 L. C. Backer, D. Manassaram-Baptiste, R. LePrell and B. Bolton, Cyanobacteria and Algae Blooms: Review of Health and Environmental Data from the Harmful Algal Bloom-Related Illness Surveillance System (HABISS) 2007–2011, *Toxins*, 2015, **7**(4), 1048–1064.

2 S. B. Watson, B. A. Whitton, S. N. Higgins, H. W. Paerl, B. W. Brooks and J. D. Wehr. Chapter 20 – Harmful Algal Blooms, in *Freshwater Algae of North America*, ed. Wehr J. D., Sheath R. G. and Kociolek J. P., Academic Press, Boston, 2015, pp. 873–920, https://www.sciencedirect.com/science/article/pii/B9780123858764000207.

3 D. G. Schmale, A. P. Ault, W. Saad, D. T. Scott and J. A. Westrick, Perspectives on Harmful Algal Blooms (HABs) and the Cyberbiosecurity of Freshwater Systems, *Front. Bioeng. Biotechnol.*, 2019, **7**, 128.

4 D. M. Anderson, P. M. Glibert and J. M. Burkholder, Harmful algal blooms and eutrophication: nutrient sources, composition, and consequences, *Estuaries*, 2002, **25**(4), 704–726.

5 I. Bertani, D. R. Obenour, C. E. Steger, C. A. Stow, A. D. Gronewold and D. Scavia, Probabilistically assessing the role of nutrient loading in harmful algal bloom formation in western Lake Erie, *J. Great Lakes Res.*, 2016, **42**(6), 1184–1192.

6 J. L. Graham, K. A. Loftin, M. T. Meyer and A. C. Ziegler, Cyanotoxin Mixtures and Taste-and-Odor Compounds in Cyanobacterial Blooms from the Midwestern United States, *Environ. Sci. Technol.*, 2010, **44**(19), 7361–7368.

7 J. A. Garcia, *The Effects of Microcystin from Harmful Algal Blooms on the Immune Functioning of Aquatic Turtles and Tadpoles*, The University of Toledo, United States – Ohio, 2022, https://www.proquest.com/docview/2322824842/abstract/A86E408FA51C4AA9PQ/1.

8 J. Hu, J. Liu, Y. Zhu, Z. Diaz-Perez, M. Sheridan, H. Royer, *et al.*, Exposure to Aerosolized Algal Toxins in South Florida Increases Short- and Long-Term Health Risk in Drosophila Model of Aging, *Toxins*, 2020, **12**(12), 787, https://www.ncbi.nlm.nih.gov/pmc/articles/PMC7763642/.

9 M. L. Wells, B. Karlson, A. Wulff, R. Kudela, C. Trick, V. Asnaghi, *et al.*, Future HAB science: directions and challenges in a changing climate, *Harmful Algae*, 2020, **91**, 101632.

10 S. J. Jacquemin, L. T. Johnson, T. A. Dirksen and G. McGlinch, Changes in Water Quality of Grand Lake St. Marys Watershed Following Implementation of a Distressed Watershed Rules Package, *J. Environ. Qual.*, 2018, **47**(1), 113–120.

11 M. M. Steffen, B. S. Belisle, S. B. Watson, G. L. Boyer and S. W. Wilhelm, Status, causes and controls of cyanobacterial blooms in Lake Erie, *J. Great Lakes Res.*, 2014, **40**(2), 215–225.

12 G. L. Boyer, Cyanobacterial Toxins in New York and the Lower Great Lakes Ecosystems, in *Cyanobacterial Harmful Algal Blooms: State of the Science and Research Needs*, ed. Hudnell H. K., Springer, New York, NY, 2008, pp. 153–165. (Advances in Experimental Medicine and Biology), DOI: 10.1007/978-0-387-75865-7_7.

13 S. M. Brittain, J. Wang, L. Babcock-Jackson, W. W. Carmichael, K. L. Rinehart and D. A. Culver, Isolation and Characterization of Microcystins, Cyclic Heptapeptide Hepatotoxins from a Lake Erie Strain of Microcystis aeruginosa, *J. Great Lakes Res.*, 2000, **26**(3), 241–249.

14 N. W. May, N. E. Olson, M. Panas, J. L. Axson, P. S. Tirella, R. M. Kirpes, *et al.*, Aerosol Emissions from Great Lakes Harmful Algal Blooms, *Environ. Sci. Technol.*, 2018, **52**(2), 397–405.

15 N. W. May, J. L. Axson, A. Watson, K. A. Pratt and A. P. Ault, Lake spray aerosol generation: a method for producing representative particles from freshwater wave breaking, *Aerosols/Laboratory Measurement/Instruments and Platforms*, 2016, https://amt.copernicus.org/preprints/amt-2016-115/amt-2016-115.pdf.

16 R. B. Pietsch, H. Grothe, R. Hanlon, C. W. Powers, S. Jung, S. D. Ross, *et al.*, Wind-driven spume droplet production and the transport of Pseudomonas syringae from aquatic environments, *PeerJ*, 2018, **6**, e5663.

17 L. E. Fleming, L. C. Backer and D. G. Baden, Overview of Aerosolized Florida Red Tide Toxins: Exposures and Effects, *Environ. Health Perspect.*, 2005, **113**(5), 618–620.

18 R. H. Pierce, M. S. Henry, P. C. Blum, S. L. Hamel, B. Kirkpatrick, Y. S. Cheng, *et al.*, Brevetoxin composition in water and marine aerosol along a Florida beach: assessing potential human exposure to marine biotoxins, *Harmful Algae*, 2005, **4**(6), 965–972.

19 W. W. Carmichael and G. L. Boyer, Health impacts from cyanobacteria harmful algae blooms: implications for the North American Great Lakes, *Harmful Algae*, 2016, **54**, 194–212.

20 C. Harb and H. Foroutan, A Systematic Analysis of the Salinity Effect on Air Bubbles Evolution: Laboratory Experiments in a Breaking Wave Analog, *J. Geophys. Res.: Oceans*, 2019, **124**(11), 7355–7374.

21 C. W. Powers, R. Hanlon, H. Grothe, A. J. Prussin, L. C. Marr and D. G. Schmale, Coordinated Sampling of Microorganisms Over Freshwater and Saltwater Environments Using an Unmanned Surface Vehicle (USV) and a Small Unmanned Aircraft System (sUAS), *Front. Microbiol.*, 2018, **9**, 1668.

22 M. R. Giordano, C. Malings, S. N. Pandis, A. A. Presto, V. F. McNeill, D. M. Westervelt, *et al.*, From low-cost sensors to high-quality data: a summary of challenges and

1362 | *Environ. Sci.: Atmos.*, 2022, **2**, 1351–1363

© 2022 The Author(s). Published by the Royal Society of Chemistry

best practices for effectively calibrating low-cost particulate matter mass sensors, *J. Aerosol Sci.*, 2021, **158**, 105833.

23 F. M. J. Bulot, S. J. Johnston, P. J. Basford, N. H. C. Easton, M. Apetroaie-Cristea, G. L. Foster, *et al.*, Long-term field comparison of multiple low-cost particulate matter sensors in an outdoor urban environment, *Sci. Rep.*, 2019, **9**(1), 7497.

24 J. Hoorman, T. Hone, T. Sudman, T. Dirksen, J. Iles and K. R. Islam, Agricultural Impacts on Lake and Stream Water Quality in Grand Lake St. Marys, Western Ohio, *Water, Air, Soil Pollut.*, 2008, **193**(1), 309–322.

25 J. González-Rocha, C. A. Woolsey, C. Sultan and S. F. J. De Wekker, Sensing Wind from Quadrotor Motion, *J. Guid. Control Dyn.*, 2019, **42**(4), 836–852.

26 J. González-Rocha, S. F. J. De Wekker, S. D. Ross and C. A. Woolsey, Wind Profiling in the Lower Atmosphere from Wind-Induced Perturbations to Multirotor UAS, *Sensors*, 2020, **20**(5), 1341.

27 P. J. Nolan, J. Pinto, J. González-Rocha, A. Jensen, C. N. Vezzi, S. C. C. Bailey, *et al.*, Coordinated Unmanned Aircraft System (UAS) and Ground-Based Weather Measurements to Predict Lagrangian Coherent Structures (LCSs), *Sensors*, 2018, **18**(12), 4448.

28 I. de Boisblanc, N. Dodbele, L. Kussmann, R. Mukherji, D. Chestnut, S. Phelps, *et al.*, Designing a hexacopter for the collection of atmospheric flow data, in *Systems and Information Engineering Design Symposium (SIEDS)*, 2014, pp. 147–152.

29 *Inspire 2 – Product Information – DJI*, DJI Official, 2022, **https://www.dji.com/inspire-2/info**.

30 J. A. Birbeck, N. J. Peraino, G. M. O'Neill, J. Coady and J. A. Westrick, Dhb Microcystins Discovered in USA Using an Online Concentration LC-MS/MS Platform, *Toxins*, 2019, **11**(11), 653.

31 R. Hanlon, S. J. Jacquemin, J. A. Birbeck, J. A. Westrick, C. Harb, H. Gruszewski, *et al.*, Drone-based water sampling and characterization of three freshwater harmful algal blooms in the United States, *Front. Remote Sens.*, 2022, **3**, 949052.

32 J. González-Rocha, L. Bilyeu, S. D. Ross, H. Foroutan, S. Jacquemin, A. Ault and D. Schmale, Application of multirotor sUAS wind profiling for resolving microscale flows in complex environments, *Environ. Sci.: Atmos.*, 2022, in revision.

33 C. M. Gotwalt, *JMP Neural Network Methodology*, SAS Inst., 2011, vol. 11.

34 M. Chen and C. Chen, Optimize Neural Network Algorithm of Missing Value Imputation for Clustering Chocolate Product Type Following "STEAMS" Methodology, *Proceedings of 35th International Conference on Computers and Their Applications*, 2020, vol. 69, pp. 230–241, **https://easychair.org/publications/open/MkGM**.

35 R. A. VanCuren, T. Cahill, J. Burkhart, D. Barnes, Y. Zhao, K. Perry, *et al.*, Aerosols and their sources at Summit Greenland – first results of continuous size- and time-resolved sampling, *Atmos. Environ.*, 2012, **52**, 82–97.

36 M. E. Dueker, G. D. O'Mullan, J. M. Martínez, A. R. Juhl and K. C. Weathers, Onshore Wind Speed Modulates Microbial Aerosols along an Urban Waterfront, *Atmosphere*, 2017, **8**(11), 215.

37 V. Pant, C. G. Deshpande and A. K. Kamra, On the aerosol number concentration-wind speed relationship during a severe cyclonic storm over south Indian Ocean, *J. Geophys. Res.: Atmos.*, 2008, **113**, D02206.

38 A. Montero, M. E. Dueker and G. D. O'Mullan, Culturable bioaerosols along an urban waterfront are primarily associated with coarse particles, *PeerJ*, 2016, **4**, e2827.

39 S. D. Ross, J. Fish, K. Moeltner, E. M. Bollt, L. Bilyeu and T. Fanara, Beach-level 24-hour forecasts of Florida red tide-induced respiratory irritation, *Harmful Algae*, 2022, **111**, 102149.

40 Y. S. Cheng, Z. Yue, C. M. Irvin, B. Kirkpatrick and L. C. Backer, Characterization of Aerosols Containing Microcystin, *Mar. Drugs*, 2007, **5**(4), 136–150.

41 H. E. Plaas and H. W. Paerl, Toxic Cyanobacteria: A Growing Threat to Water and Air Quality, *Environ. Sci. Technol.*, 2021, **55**(1), 44–64.

42 B. Kirkpatrick, L. E. Fleming, J. A. Bean, K. Nierenberg, L. C. Backer, Y. S. Cheng, *et al.*, Aerosolized red tide toxins (brevetoxins) and asthma: continued health effects after 1h beach exposure, *Harmful Algae*, 2011, **10**(2), 138–143.

43 J. Sutherland, The detection of airborne anatoxin-a (ATX) on glass fiber filters during a harmful algal bloom, *Lake Reservoir Manage.*, 2021, **37**(2), 113–119.

44 N. E. Olson, M. E. Cooke, J. H. Shi, J. A. Birbeck, J. A. Westrick and A. P. Ault, Harmful Algal Bloom Toxins in Aerosol Generated from Inland Lake Water, *Environ. Sci. Technol.*, 2020, **54**(8), 4769–4780.

© 2022 The Author(s). Published by the Royal Society of Chemistry

Environ. Sci.: Atmos., 2022, **2**, 1351–1363 | **1363**